Journal of Applied Physics

Hot-carrier enhanced light emission: The origin of above-threshold photons from electrically driven plasmonic tunnel junctions

Cite as: J. Appl. Phys. **128**, 233105 (2020); https://doi.org/10.1063/5.0024392
Submitted: 06 August 2020 • Accepted: 02 December 2020 • Published Online: 21 December 2020

Yunxuan Zhu, Longji Cui and Douglas Natelson

AIP Publishing

Journal of Applied Physics ARTICLE scitation.org/journal/jap

Hot-carrier enhanced light emission: The origin of above-threshold photons from electrically driven plasmonic tunnel junctions

Cite as: J. Appl. Phys. **128**, 233105 (2020); doi: 10.1063/5.0024392
Submitted: 6 August 2020 · Accepted: 2 December 2020 ·
Published Online: 21 December 2020

Yunxuan Zhu,[1] Longji Cui,[2,3] and Douglas Natelson[1,4,5,a)]

AFFILIATIONS

[1]Department of Physics and Astronomy, Rice University, Houston, Texas 77005, USA
[2]Paul M. Rady Department of Mechanical Engineering, University of Colorado, Boulder, Colorado 80309, USA
[3]Materials Science and Engineering Program, University of Colorado, Boulder, Colorado 80309, USA
[4]Department of Electrical and Computer Engineering, Rice University, Houston, Texas 77005, USA
[5]Department of Materials Science and Nanoengineering, Rice University, Houston, Texas 77005, USA

Note: This paper is part of the Special Topic on Hot Electron Physics and Applications.
[a)]**Author to whom correspondence should be addressed:** natelson@rice.edu

ABSTRACT

Understanding the origin of above-threshold photons emitted from electrically driven tunnel junctions ($\hbar\omega > eV_b$ with V_b being the applied voltage bias) is of current interest in nano-optics and holds great promise to create novel on-chip optoelectronic and energy conversion technologies. Here, we report experimental observation and theoretical analysis of above-threshold light emission from electromigrated Au tunnel junctions. We compare our proposed hot-carrier enhanced light emission theory with existing models, including blackbody thermal radiation, multi-electron interactions, and an interpretation involving finite temperature effects. Our study highlights the key role of plasmon-induced hot carrier dynamics in emitting above-threshold photons and the need to further explore the underlying mechanisms and optimization of upconversion effects in plasmonically active nanostructures.

I. INTRODUCTION

The study of plasmon-enhanced light emission in electrically driven tunnel junctions is an ongoing research topic at the interface of nano-optics and nano-electronics. Nanometer-scale tunneling junctions provide an ideal experimental platform to test the physical behavior of plasmonic excitations and associated hot-carrier dynamics at the extreme nanoscale,[1–6] extending the current experimental capabilities in probing electronic, thermal, and mechanical properties at the fundamental limit of nanodevices and nanojunctions.[7–13] Light emission from tunnel junctions[14] has long been connected to localized surface plasmons (LSPs) confined in the tunneling gap. LSPs can be excited by inelastically tunneling electrons and subsequently decay radiatively into far field light emission, which features photon energies below the energy scale of individual tunneling electrons (i.e., below-threshold light emission with $\hbar\omega \leq eV_b$).[4,14–20] Such emission can also be realized via propagating surface plasmons in resonant antenna structures.[21–23] Much effort has been devoted over the past decade to improve the electricity-to-light energy conversion efficiency (i.e., photon yield) by optimizing the plasmonic properties of tunnel junctions and associated plasmonic nanostructures.[16,18,24–26]

In contrast to the study of below-threshold light emission, recent experimental observations of above-threshold light emission[27–38] ($\hbar\omega > eV_b$ with even $2\,eV_b$ or $3\,eV_b$ of photon emission observed), in both STM and nanofabricated planar tunnel junctions, have triggered great interest. The underlying physics remains an open question, while the energetic upconverted photons could be potentially leveraged in numerous applications such as on-chip subwavelength photon sources,[21,39] photochemistry,[40–42] plasmon-enhanced surface spectroscopy,[43–45] and sensing.[46–48]

A number of competing theoretical models have been put forward to understand the origin of above-threshold light emission.

During the inelastic single electron tunneling process, an initial state electron located at the band edge [eV_b away from E_F, Fig. 1(a)] can gain an excess energy by the thermal broadening of the Fermi-Dirac distribution at a finite lattice temperature, creating a photon with an energy higher than eV_b by a few k_BT (~26 meV at room temperature).[38] By contrast, higher-order coherent multi-electron interactions, either mediated by a plasmon excitation[36] or via an Auger-like process followed by hot hole cascades,[49] are also expected to play a role in facilitating energy upconversion of tunneling electrons, leading to photon emission with significantly higher energies extending to $2eV_b$ and above, as shown in Fig. 1(b).

Rather than the coherent interactions of multiple tunneling electrons, another incoherent "many-electron" interaction mechanism to explain the observed above-threshold light emission is based on spontaneous blackbody thermal radiation of the hot electron gas.[28,29,35] As illustrated in Fig. 1(c), tunneling electrons can reach a steady-state Boltzmann-like distribution with an effective temperature above 1000–2000 K due to the energy redistribution rate within the electronic system via electron–electron scattering enormously surpassing the cooling rate through electron–phonon scattering. If such quasi-thermalization can take place, at such a high non-equilibrium effective electronic temperature, the broadband spontaneous thermal radiation of the hot electron subsystem naturally leads to the emission of above-threshold photons, with an emission spectrum modified from the free-space Planck form by the plasmon-enhanced local photonic density of states of the nanostructure.

Recently, we proposed a new above-threshold light emission model based on plasmon-induced hot-carrier generation and recombination.[30] It is known that hot carriers are generated via Landau damping of surface plasmons,[5] and that those LSPs can be excited by both electronic and optical means. As shown in Fig. 1(d), LSPs are electrically excited by nearly continuously arriving inelastic tunneling electrons (time interval between consecutive tunneling events $\sim e/I = 0.16$ ps at $10\,\mu A$). These LSPs decay nonradiatively into hot electron–hole pairs and through electron–electron scattering form a steady-state distribution as the generation rate of hot carriers outpaces the decay rate. Broadband light emission including above-threshold photons is then produced as a consequence of recombination of hot electrons and hot holes enhanced by the LSP-modified density of states for photons. A major difference between this hot-carrier based model and the blackbody radiation model is the role of LSPs in the generation of the hot carriers. While the emission spectrum in both theories reflects the local density of states of plasmonic excitations, LSPs are key to further enhancing light emission in the hot-carrier model via mediating hot-carrier dynamics and introducing a dramatically different voltage dependence of light emission, which we will discuss in detail below.

In this work, we report experimental measurements of above-threshold light emission in electromigrated planar Au tunnel junctions and compare the data with expectations of the various models described above. Our modified normalization analysis approach based on the blackbody radiation model further validates the plasmon-induced hot-carrier picture of the observed above-threshold light emission. By comparing our results with other theoretical models, our study emphasizes the contribution of hot-carrier dynamics in plasmonic upconversion light emission. We also

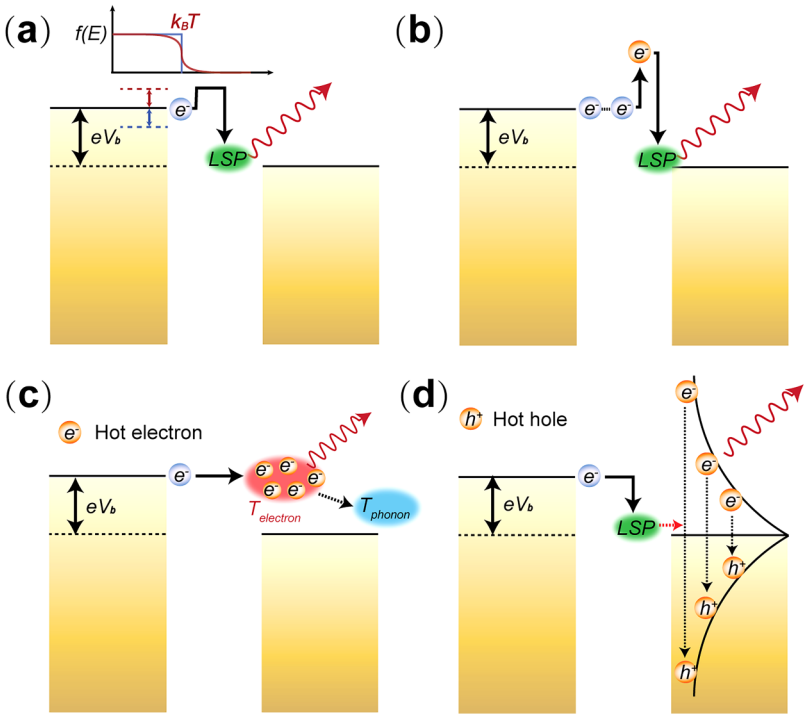

FIG. 1. Schematics of different candidate light emission mechanisms. (a) During the inelastic tunneling process, an electron can gain excess energy due to the thermal smearing of the Fermi-Dirac distribution, creating a higher energy LSP that results in the above-threshold light emission. (b) Multiple electrons collaboratively tunnel coherently through the junction via a higher order process, scattering off a high energy LSP which subsequently generates the above-threshold light emission. (c) Heat dissipation after inelastic electron tunneling facilitates the formation of the hot electron subsystem, which decouples from the lattice. Above-threshold light emission then comes from the spontaneous blackbody thermal radiation of the electrons. (d) Electrically excited LSPs nonradiatively decay into hot electron–hole pairs. Radiative recombination of hot electrons and holes, which are sustained in a steady-state distribution, leads to the above-threshold light emission.

discuss further experimental and theoretical research directions on this topic.

II. EXPERIMENTAL RESULTS

A home-built Raman spectroscopy setup is employed to perform the light emission measurements, as described in detail in our previous work.[30] Arrays of Au nanowires with different aspect ratios (600 nm or 60 nm long, 100 nm wide, 18 nm thick) are fabricated on the SiO_2/Si wafer using e-beam lithography and evaporation, with an ultrathin adhesion layer of Cr (1 nm). Samples are thoroughly cleaned using multiple cycles of oxygen plasma to minimize contamination during the preparation process before mounting into the high vacuum cryostat ($\sim 5 \times 10^{-9}$ Torr and 5 K). Emitted photons from the biased tunnel junction were collected through free space optics and directed into a Si CCD spectrometer.

To create a stable tunneling gap under various biases, we apply an electromigration protocol[50] to break the Au nanowire. In brief, multiple voltage scanning loops are slowly applied into nanowires to introduce the electromigration process. Each loop is ended at a stop bias signaled by a small conductance drop to a preset value. An atomic-scale tunneling gap is formed once the zero-bias conductance of the nanowire jumps below the quantum conductance ($G_0 = 2e^2/h$). Subsequent optical emission measurements are conducted at the voltage biases that are below the highest electromigration value and at cryogenic temperatures, to discourage further enlarging of the nanogap.

Polarization and spectral characteristics of the emitted photons can be obtained from spectroscopic measurements by integrating a polarizer into the Raman setup. As can be seen in Fig. 2, representative polarization-spectral contour plots of light emission ranging from 1.2 eV-2.2 eV reveal delicate mode structures of the LSP resonances modulating the total spectral properties [Figs. 2(a) and 2(d) are for 600 nm and 60 nm long nanowires, respectively]. Specifically, 0° and 90° polarization spectra were extracted from the contour plots and plotted separately in Figs. 2(b) and 2(e). It can be seen that while the emission peak at around 1.3 eV is shown in both cases (long and short nanowires), the 1.7 eV peak is only imprinted at 90° for the 600 nm long nanowire. This is a consequence of the hybridization of the transverse plasmon mode from the nanowire and the dipolar tip mode from the atomic-scale tunneling gap.[51,52] In Fig. 2(b) for the 0-degree polarization, there is a small peak at 1.9 eV not seen in the 60-nm Au/Cr junctions. We believe there are multiple possible explanations for the small peak at 1.9 eV for 0-polarization: one is the charge transfer plasmon existing in electrically coupled plasmonic nanostructures; another is a higher order plasmonic mode. Given the complex and large device-to-device variations in the atomic structure of the tunnel junction after electromigration, it is possible that the 60 nm device we measured may not exhibit such a

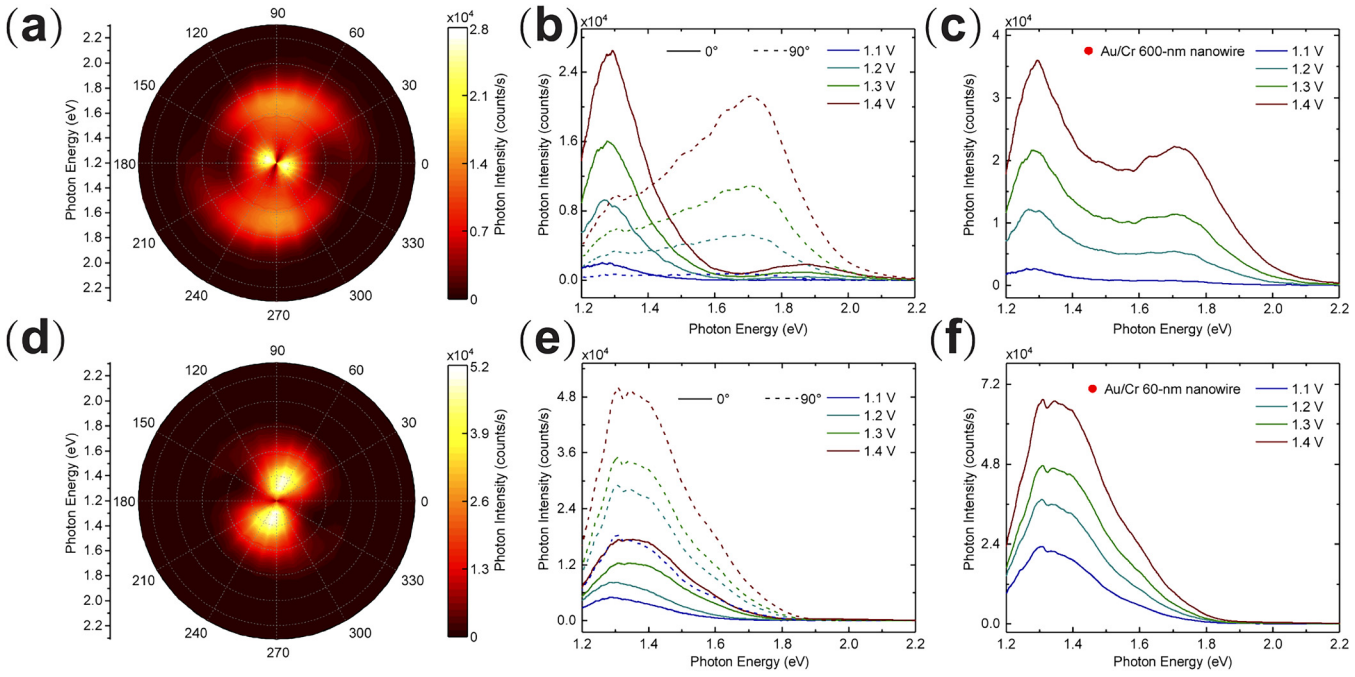

FIG. 2. Spectral and polarization-dependent light emission measurements of tunnel junction devices with different nanowire aspect ratios. (a) and (d) Polar contour plot of the polarization-dependent light emission for the Au/Cr tunnel junction with 600-nm-long nanowire (0.27 G_0 zero-bias conductance, top) and with 60-nm-long nanowire (0.19 G_0 zero-bias conductance, bottom), respectively. The radial coordinate is the photon energy, while zero-degree polarization is defined as lying along the nanowire dirction. (b) and (e) Extracted 0° (along the nanowire) and 90° (perpendicular to the nanowire) polarization spectra in (a) and (d). (c) and (f) Polarization-free emission spectra obtained from the summation of 0° and 90° spectra at different biases in (b) and (e).

peak, or the relative weak plasmonic resonance is strongly attenuated in this device compared to the one in Fig. 2(b). Polarization-free emission spectra in Figs. 2(c) and 2(f) from the summation of respective 0° and 90° spectra exhibit a photon flux gain when increasing the voltage. The nontrivial polarization features and their device-to-device variation demonstrate that engineering the LSP resonances by different nanostructure geometries greatly influence the emission spectral shape of the voltage-tunable nanoscale light source.

In conducting the light emission experiments, we also perform multiple-step electromigration on individual tunnel junctions to study the effects of minor geometric changes. Specifically, the tunneling gap is further enlarged by a second electromigration step via applying a higher voltage bias into the nanowire. It can be seen that an enlarged gap features much smaller zero-bias conductance (typically by an order of magnitude), as shown in Figs. 3(a) and 3(b). After the second electromigration, higher biases for the optical spectroscopic measurements are preferable due to the smaller tunneling current at a given bias, resulting in a considerable drop in photon intensity. For example, the peak emission intensity under similar voltage [1.4 eV in Fig. 3(a) and 1.6 eV in Fig. 3(b), respectively] for the same junction before and after the second electromigration exhibits a nearly 20 times amplitude decrease, while the current only drops by a factor of 6, suggesting a nonlinear behavior in the photon output. Furthermore, the same junction after the second electromigration shows a significant spectral shape variance, indicating that the modification of LSP resonance which varies with the gap distance[53,54] greatly affects the light emission.

Here, we note that all measurements for the Au/Cr junction presented here exhibit a smooth onset of emitted photons as a function of frequency, whereas in our previous work[30] the Au/Cr junction (after the multi-step electromigration procedure) shows a sharp bias dependent onset of excitation frequency (cut-off frequency at $\hbar\omega = eV_b$). To clarify, this distinction results from the magnitude of the tunneling current in the junction. If tunneling current is high enough, meaning the electrical conductance is also high, the hot carrier generation rate (proportional to the current) is higher than its relaxation rate, and a steady-state energy distribution of hot carriers can then be formed, with above-threshold photons consequently generated through radiative recombination of hot carriers. In contrast, if the tunneling current is very small, no steady-state hot carrier distribution can be formed because the tunneling rate of electrons is insufficient to sustain that. Light emission in this latter case will be limited to the radiative decay of LSP modes excited by single-electron inelastic tunneling processes, and hence have a cutoff.

III. THEORETICAL ANALYSIS AND COMPARISON WITH EXISTING MODELS

A. Normalization analysis and hot-carrier light emission model

As shown in Fig. 3, we have found that spectra from the same junction configuration exhibit similar shapes under different biases, suggesting a voltage-independent LSP resonance-based multiplication factor is embedded in all spectra. Inspired by this observation and a previous semi-logarithmic intensity analysis,[35] we removed the multiplication factor by applying a normalization approach (i.e., dividing a reference spectrum under arbitrary bias). Such normalization is valid based on the hot electron thermal emission model with the density of states modified by the LSP modes,[35] where normalization can effectively remove the frequency

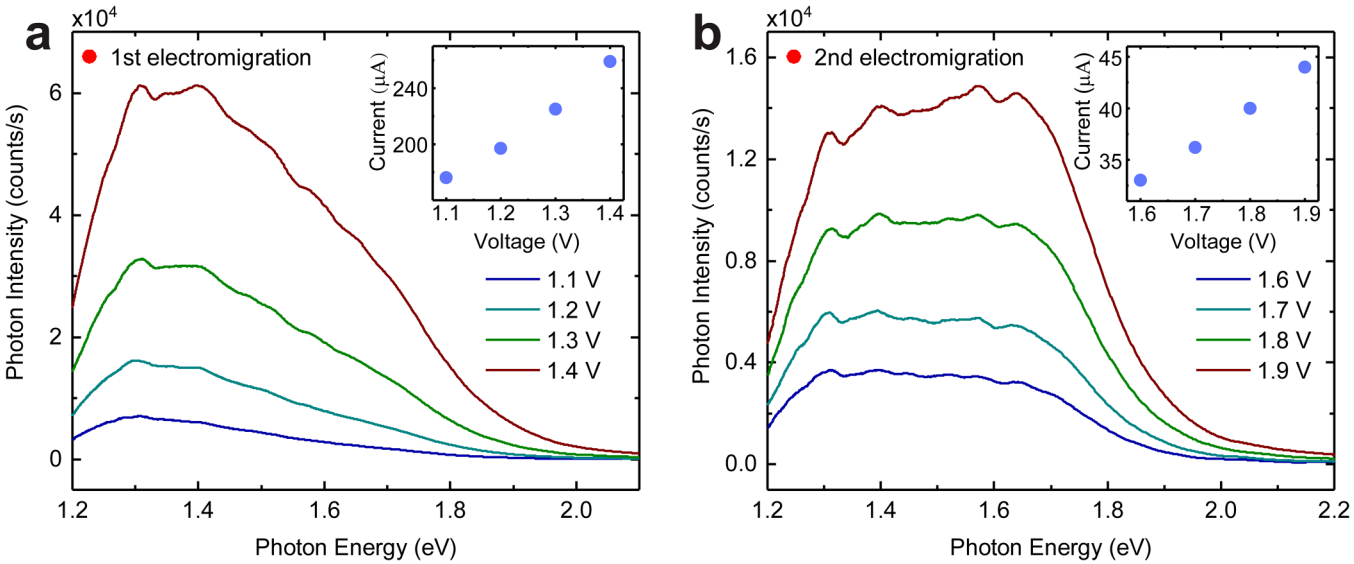

FIG. 3. Spectral measurements after two-step controlled electromigration. (a) Measured spectral light emission intensity after first electromigration with 0.31 G_0 zero-bias conductance from 1.1 V to 1.4 V. (b) Measured spectral light emission intensity after second electromigration with 0.02 G_0 zero-bias conductance from 1.6 V to 1.9 V. Insets in (a) and (b) show the corresponding electrical transport measurement after each electromigration.

dependent plasmon-modified density of states, leaving the Boltzmann factor only. We chose the spectrum measured under the highest voltage as the reference to normalize all other spectra measured at different voltage biases. As can be seen in Figs. 4(a) and 4(b) [normalized spectra for the curves in Figs. 3(a) and 3(b), respectively], the reduced spectrum, when plotted on the logarithmic scale, clearly demonstrates an excellent linear dependence with photon energy.

The linear dependence with the energy on a logarithmic scale is reminiscent of the Boltzmann energy distribution ($e^{-\hbar\omega/k_B T_{eff}}$) in statistical physics, where T_{eff} is the effective hot-carrier temperature of the physical system. Here, we define an effective temperature via a Boltzmann factor to describe the voltage dependent behavior in the normalized curves,

$$U_{Norm}(V_b, \omega) \propto e^{-\frac{\hbar\omega}{k_B T_{eff}}}, \quad (1)$$

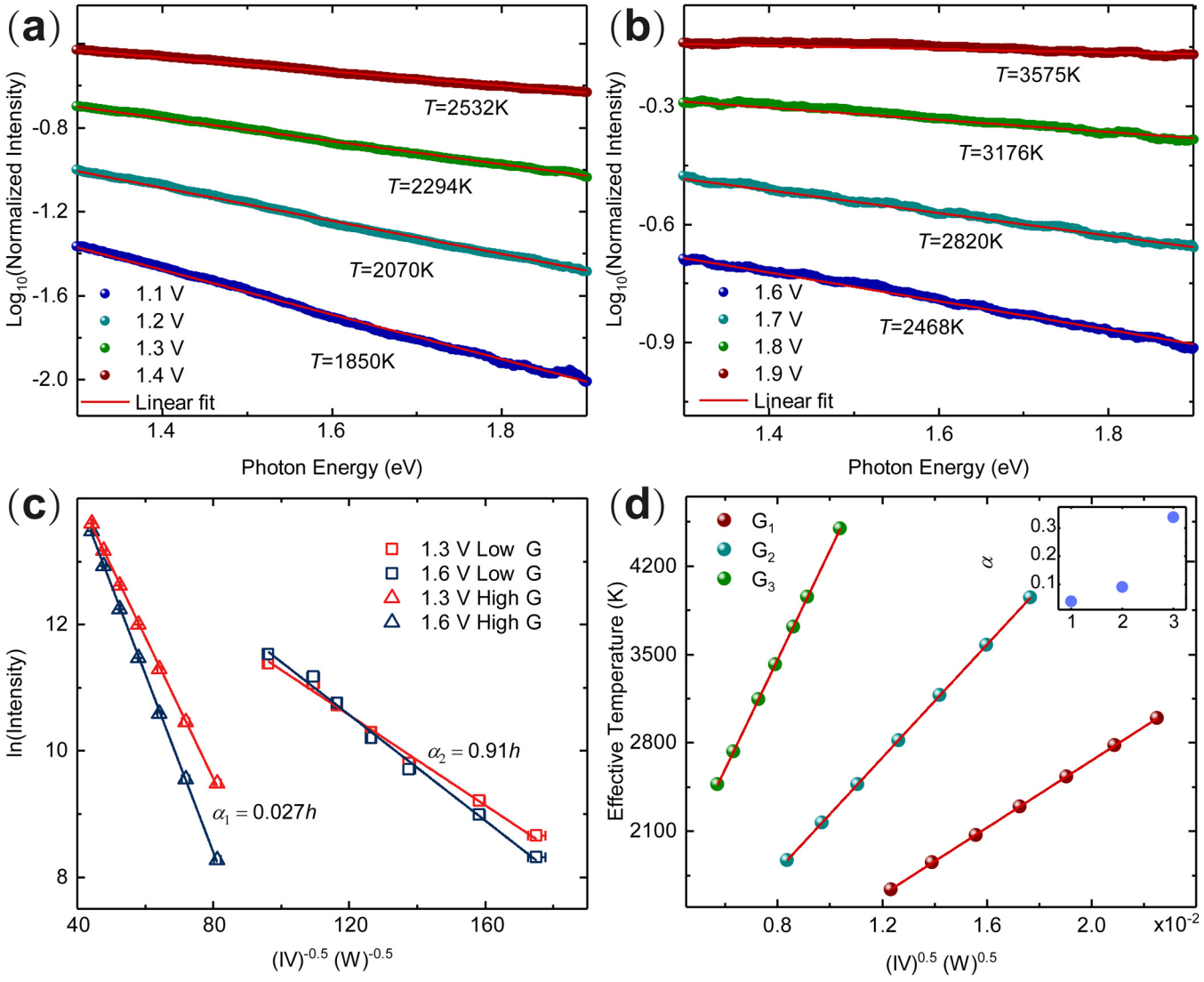

FIG. 4. Testing a purely hot electron gas model via normalization analysis and α extraction of the measured data in Fig. 2. (a) Normalized curve after dividing the 1.6 V reference for the first electromigration in Fig. 2(a). Effective hot-carrier temperature of each curve is extracted by linear fitting, same for (b). (b) Normalized curve after dividing the 2.0 *V* reference for the second electromigration in Fig. 2(b). (c) α extraction for data in (a) and (b) by linear fitting the summed photon intensity vs reciprocal of the square root of electrical power on a logarithmic scale. Values shown in the figure have already been divided with the respective photon energy. (d) Calculated effective temperature using extracted α for (a) and (b), with an additional line corresponding to a third electromigration. The inset shows the α values after each electromigration. Note that in the proposed hot electron gas picture, α is supposed to be dependent only on the material and is not expected to vary.

where the $U_{Norm}(V_b, \omega)$ is the normalized spectrum as a function of bias V_b and photon frequency ω, and k_B is Boltzmann constant. The slope K of each linear normalization curve in Fig. 4 then has the form

$$K = -\left(\frac{1}{k_B T_{eff}^{i}} - \frac{1}{k_B T_{eff}^{ref}}\right), \tag{2}$$

where T_{eff}^{i} is the effective temperature for the current curve and T_{eff}^{ref} is for the reference curve.

Here, it is to be noted that proper caution is needed to define an effective temperature of any driven, non-equilibrium system.[55] Our toy model (as described in detail in our previous work[30]) is based on a recently developed, full quantum mechanical jellium model to understand hot carrier relaxation dynamics in metallic nanoparticles.[56] It describes that the non-equilibrium hot carriers excited via non-radiative decay of LSPs form a steady-state distribution that is sustained during continuous excitation of LSPs and hot-carrier generation. The linear voltage dependence of the effective hot-carrier temperature can be well explained by the plasmon-induced hot carrier relaxation model.[56] Hot carriers in the steady state distribution are generated via electrically driven LSPs whose energy scale are set by the bias ($E_F \pm eV_b$ where E_F is the Fermi level).[56] Subsequent hot carrier dynamics then enable the derivation of the effective hot-carrier temperature as a function of the electrical bias and a material-dependent factor which is deeply connected to the carrier mean lifetime of the metallic material according to the model. This inference is consistent with the observed positive correlation relationship between the fitted T–V slope and material plasmonic properties.[30] The radiative recombination of the hot carriers then leads to the substantial above-threshold light emission, with LSP resonances imprinted as a common multiplication factor particular to each device. Total spectral density for the light emission is thus given by

$$U(V_b, \omega) \propto I^a \rho(\omega) \hbar\omega e^{-\frac{\hbar\omega}{\beta e V_b}}, \tag{3}$$

where I is the tunneling current, V_b is the bias, a is a power factor which is always larger than 1 from measurements,[30] indicating the nonlinear behavior in the above-threshold light emission, $\rho(\omega)$ gives the local photon density of states which is deeply connected to the LSP resonances, and β is a factor which decreases as the material becomes plasmonically lossy.

B. Spontaneous blackbody thermal radiation model

Comparison of the normalization results under different gap distances produced from multi-step electromigration can provide important insights into whether the dissipative heating or the plasmon-induced nonradiative decay is the dominant mechanism in forming the hot carriers. Here, we note that by "dissipative heating" we are specifically discussing about Joule heating generated by the input electrical power. In the former Joule heating-induced hot electron picture, the redistribution of the energy among carriers results in an increase of their effective electronic temperature T_{eff} that thermally decouples from the lattice degrees of freedom. This T_{eff}, when including the energy dissipation via surface collisions within the nano-constriction, is expected to be proportional to the square root of the injected electrical power in the high temperature limit,[28,29,35]

$$k_B T_{eff} = \sqrt{\alpha P_e + (k_B T_L)^2} \approx \sqrt{\alpha P_e}, \tag{4}$$

where P_e is the dissipated electrical power (i.e., IV_b), T_L is the lattice temperature that will be slightly increased due to Joule dissipation but is much smaller than the effective temperature of hot electron gas, α is a factor that determined by the nanowire geometry and the material only,[35]

$$\alpha = \frac{4k_B}{L^{\frac{3}{5}} m\pi \sqrt{2b\frac{E_F}{M\hbar^3}}}, \tag{5}$$

where L is the mean-free path for electrons to collide with the surface, E_F is the Fermi energy, m and M are, respectively, the mass of electrons and atoms, and b is the electronic heat conductivity coefficient. It can be directly inferred from the derivation that α will not depend on the gap distance, making the aforementioned multi-step electromigration method an effective way in discerning the hot carrier origin.

To show this, we employed a linear fitting analysis similar to prior efforts[28,35] to analyze the data in Fig. 2 to extract α. As can be seen in Fig. 4(c), we integrated the photon intensity at two peak positions (1.3 eV and 1.6 eV) and plotted them on a logarithmic scale vs the reciprocal of the square root of electrical power. The slope of the linear fitting results for the data points then contains α, which is given by[35]

$$\ln(U(V_b, \omega)) = \ln(\rho(\omega)\hbar\omega) - \frac{\hbar\omega}{\sqrt{\alpha P_e}}. \tag{6}$$

After fitting the data points and dividing the respective photon energy in Eq. (6), the extracted α shows a nearly 3× difference between the low and high conductance case, which is not compatible with the dissipative heating model. We further calculate T_{eff} using Eq. (4) taking T_L as 5 K (substrate temperature in our measurement) and plotting T_{eff} in Fig. 4(d) with an additional line corresponding to a third electromigration of the same junction. The nearly 10× difference between the highest and the lowest α values indicates that a similar range of the effective electronic temperature (~2000 K to 4000 K) is attainable even at the same electrical power. Hence, these findings, combined with the lack of correlation between T_{eff} and $\sqrt{IV_b}$ when averaged over an ensemble of junctions of the same material, suggest that the plasmon-induced hot carrier generation mechanism would dominate in a plasmonic resonant nanostructure (as in the present experiments), while in the non-resonant case, the spontaneous thermal emission is likely to be the main mechanism for above-threshold light emission.[29]

C. Coherent multi-electron interactions

Another normalization analysis approach ("second normalization" in the following discussion) has also be introduced to test for the coherent multielectron tunneling mechanism in the above-threshold light emission.[36] According to the coherent multielectron theory,[36,57–59] multiple electrons could collaboratively tunnel through the barrier via a higher order process, scattering off a high energy LSP (which can be modeled as a dampened LC circuit) and subsequently leading to the above-threshold light emission. A large tunneling current ($I > 10\,\mu$A) is preferable to enable a reliable detection of sufficient multielectron light emission with photon energy extending to $2\,eV_b$ and above, since the quantum efficiency of higher order processes is significant lower compared to the single electron event.[32] Such light emission can be phenomenologically described as the combination of two separable parts, with one coming from the LSP contribution and another from the electron dynamics. Compared to the hot carrier case, current fluctuation (shot noise) spectral density[57–59] is used to parameterize the electron dynamics instead of the steady state carrier distribution. The total spectral intensity is hence a summation of contributions from different orders of interaction between the current fluctuation and plasmon resonance,[36]

$$U(V_b, \omega) = U_{1e}(V_b, \omega) + U_{2e}(V_b, \omega) + U_{3e}(V_b, \omega) + \cdots, \tag{7}$$

where $U_{ne}(V_b, \omega)$ represents the nth order contribution from electron–plasmon interaction. Since higher order electron–plasmon interaction probabilities decay rapidly with n, very high order terms in Eq. (7) can be ignored. Expressions for $1e$, $2e$, and $3e$ process are given by[36]

$$U_{1e}(V_b, \omega) = R_0 \tilde{g} \rho(\omega) \tilde{S}(V_b, \omega), \tag{8}$$

$$U_{2e}(V_b, \omega) = R_0 \tilde{g}^2 \rho(\omega) \int_{\hbar\omega - eV_b}^{eV_b} d\varepsilon \rho(\varepsilon) \tilde{S}(V_b, \varepsilon) \tilde{S}(V_b, \hbar\omega - \varepsilon), \tag{9}$$

$$U_{3e}(V_b, \omega) = R_0 \tilde{g}^3 \rho(\omega) \int_{\hbar\omega - 2eV_b}^{eV_b} d\varepsilon \int_{\hbar\omega - eV_b - \varepsilon}^{eV_b} d\varepsilon' \times \rho(\varepsilon) \tilde{S}(V_b, \varepsilon) \tilde{S}(V_b, \varepsilon') \rho(\varepsilon') \tilde{S}(V_b, \hbar\omega - \varepsilon - \varepsilon'), \tag{10}$$

where R_0 is a common factor, $\tilde{g}$ is the coupling coefficient between the current and the plasmon, $\rho(\omega)$ corresponds to the LSP resonance, $\tilde{S}(V_b, \omega) = S(V_b, \omega)G$ where $S(V_b, \omega)$ is the shot noise spectrum through non-interacting conductance channels, and G is the conductance of the junction.[36] Due to the quantized nature of the coherent multielectron process, after removing the part of LSP contribution, a slope discontinuity, which is the signature of discretized contribution from different orders of interaction, would occur at each corresponding energy level ($h\nu = neV_b$).[36] Based on the above equation and rigorous mathematical derivation,[36] $\rho(\omega)$ can be removed in every term in Eq. (7) by dividing by the reference curve and multiplying the summation of different orders of current fluctuation in Ref. 36,

$$N_V(\hbar\omega) = \frac{U_V(V_b\,, \omega)}{U_{V_R}(V_R, \omega)} \left(1 - \frac{\hbar\omega}{eV_R}\right), \tag{11}$$

where $U_{V_b}(V_b\,, \omega)$ is the spectrum under bias V_b, and V_R is the voltage for the reference spectrum. One may notice that only the first order shot noise factor[60] in Eq. (7) $(1 - \hbar\omega/eV_R)$ has been involved into the normalized expression as the current fluctuation term for the reference. Unlike the hot carrier mechanism, where the simple Boltzmann distribution leads to the elegant linear behavior after normalization, the more complicated electron–plasmon interaction for second and third orders in Eqs. (9) and (10) inspires one to use the noise spectral density, which is proportional to $(1 - \hbar\omega/eV_R)$ as the approximation for the reference curve. This approximation is justified when the reference voltage is sufficiently higher than other curves ($\Delta V_b \sim 1$V).[36] Hence, when a sufficient higher reference voltage has been satisfied, the presence of kinks at neV_b after the normalization defined in Eq. (11) is a strong indicator for the dominance of the coherent multielectron mechanism.[36]

We then conducted controlled electromigration and measurement on the same junction to examine the role of multielectron interactions in above-threshold light emission from our studied Au tunnel junctions. Since it is difficult to maintain the junction stability at a same gap distance (same LSP resonance) across a large range of bias ($\Delta V_b \gg 1$V), we used two spectra curves as references to obtain reliable normalization results. One is obtained at a fixed gap distance with the highest bias, and another one is measured under a much higher bias than the previous one after enlarging the gap by further electromigration. As shown in Fig. 5(a), complete optical measurements from 1.5 V to 2.0 V are performed at one gap distance (1st electromigration), followed by a slowly careful electromigration (2nd electromigration) to enlarge the tunneling gap and measure the reference spectrum at 2.5 V. The normalized spectrum, both for 2.0 V and 2.5 V references, exhibit a smooth crossover at $1\,eV_b$ on a logarithmic scale [Figs. 5(b) and 5(c)]. Further control experiments conducted at various substrate temperatures (not shown) continue to show no signature of kink-like features at the photon energies corresponding to integer multiples of the bias scale.[30] Though finite lattice temperature effects can smear the $2\,eV_b$ kink, the abrupt transition should always remain sharp and prominent at $1\,eV_b$ where we investigate.[36] The lack of kinks at integer multiples of the bias strongly suggests that the multielectron mechanism is not likely to dominate over the hot carrier generated above-threshold light emission in our experiments.

D. Finite temperature effects

We continue to test for finite temperature effects in the observed above-threshold light emission. The well-established low current, below-threshold light emission picture states that the emitted photons originate from the contribution of LSP resonances and the electronic shot noise in the tunnel junction due to a single electron transport process,[38,61]

$$U(V_b, \omega) \propto \rho(\omega) \times \frac{e}{2\pi} \left[I(eV_b - \hbar\omega) \coth\left(\frac{eV_b - \hbar\omega}{2k_B T}\right)\right], \tag{12}$$

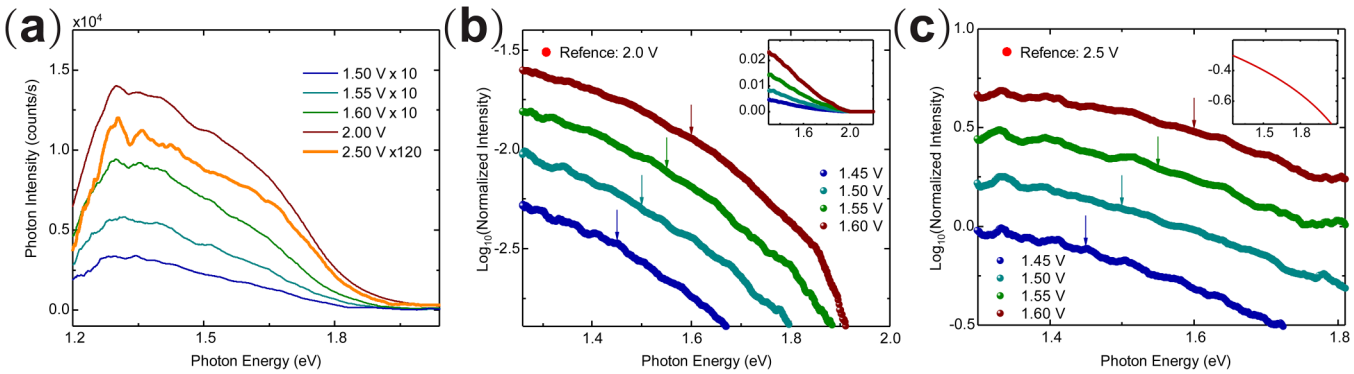

FIG. 5. Testing for coherent multielectron processes via the second normalization method. (a) Measured spectral light emission intensity from 1.5 V to 2.0 V at a same gap distance (0.06 G_0 zero-bias conductance). The bold orange line is obtained after a further electromigration with 0.002 G_0 zero-bias conductance at 2.5 V. (b) Normalized curves are plotted on the logarithmic scale after applying the second normalization method with 2.0 V selected as a reference. Colored arrows indicate corresponding photon energies at $\hbar\omega = eV$. The inset shows the normalized data plotted on the linear scale. (c) Same as (b) but with 2.5 V taken as a reference. The inset plotted the current noise spectral density $(1 - \hbar\omega/eV_r)$ on the logarithmic scale with $V_r =$ 2.5 V. The lack of any pronounced kink at the indicated energies argues against the coherent multielectron model in this case.

where I is the tunneling current of the junction. When approaching the zero temperature limit, this simplifies to the form in Eq. (13) with a clear energy cutoff at $\hbar\omega = eV_b$,[38] which corresponds to the below-threshold light emission,

$$U(V_b, \omega) \propto \rho(\omega) \times \frac{eV_b}{2\pi R_{eff}} \left(1 - \frac{\hbar\omega}{eV_b}\right), \tag{13}$$

where R_{eff} is the junction resistance. At a modest lattice temperature (e.g., 100 K), the spectral density of the electrical noise rises to a finite non-zero value at the cutoff threshold, as a result of thermal smearing of the Fermi-Dirac distribution near the Fermi energy. After coupling to the characteristic LSP energies, the generated far field light emission features a spectral tail extending beyond eV_b. To test for this mechanism, a scaling method which removes the effect of current noise has been applied[38] by normalizing the photon intensity with the numerically calculated current noise spectra. Such normalization is justified given that above-threshold light emission under this model can be expressed as a direct multiplication between LSP modes and a current noise spectrum, hence by scaling the noise spectrum one can directly investigate the fixed LSP modes for the same STM tip. As can be derived from Eq. (12), all the scaled spectra below the threshold collapse onto a single curve, indicating intrinsic the LSP contribution.

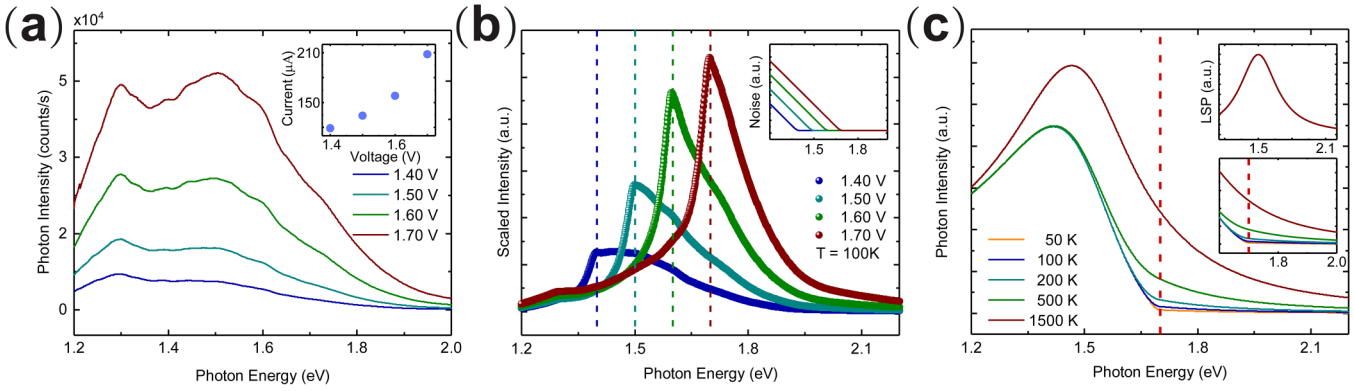

FIG. 6. Scaling analysis based on the finite lattice temperature above-threshold mechanism. (a) Measured spectral light emission intensity from 1.4 V to 1.7 V with 0.16 G_0 zero-bias conductance. The inset shows the corresponding electrical transport measurement for the junction. (b) Scaled spectra using the expected current noise spectral density at 100 K as a reference, which is plotted in the inset. (c) Calculated total spectrum using a Lorentzian line shape LSP (upper inset) with a peak energy centered at 1.5 eV and noise spectrum biased at 1.7 V with a lattice temperature ranged from 50 K to 1500 K. Dotted red line marks the bias position. The bottom inset is a magnified view for (c) near the 1.7 V bias. The fact that unphysically large equilibrium temperatures (for the current noise smearing) would be needed for this model to describe the observed above-threshold emission strongly suggests that this is not the relevant mechanism at work in this device.

Similarly, we performed the scaling analysis following previous work[38] on a representative measurement to identify whether this finite temperature effect in current noise is the main above-threshold emission mechanism (Fig. 6). Parameters used for the calculation of the noise spectra at 100 K are the mean barrier height of Au ($\bar{\phi} = 5.1$ eV)[38] and the tunnel gap distance ($d = 0.20$ nm obtained from the $I - V$ curve fitting of the tunnel junction using the Simmons model[62]). However, as can be seen from Fig. 6(b), the scaled spectra exhibit significant deviations below the threshold set by the voltage, indicated by a colored dotted line. This suggests that simply assuming current fluctuations at an elevated lattice temperature might be inconsistent with the data. We proceed further to calculate the total light emission spectrum by assuming a Lorentzian shape LSP spectra with a peak energy centered at 1.5 eV [Fig. 6(a)]. It can be seen in Fig. 6(d) that significant amount of the above-threshold light emission comparable to our experiment is only possible at an extremely high lattice temperature (>1500 K). Such a dramatically high equilibrium temperature (different from the non-equilibrium hot-carrier temperature discussed above) would inevitably result in the melting of the nanostructure, inducing instability to the electromigrated tunneling gap. However, in performing measurements, we continuously monitor the tunneling current flowing across the junction and no discernible change in the conductance or light emission characteristics is observed. Therefore, these observations lead to the conclusion that the thermal current fluctuations cannot be the dominant mechanism for the above-threshold light emission for junctions operating under a high current regime ($I > 100\,\mu$A). By contrast, other investigators have found that this mechanism dominates the emission spectra of low zero-bias conductance junctions ($<\sim 10^{-3}\ G_0$).[14,27]

Here, we emphasize that three different normalization methods have been applied to the light emission spectra throughout the paper, with each method corresponding to a specific above-threshold light emission model. All three methods are based on rigorous mathematical derivation and all intend to investigate either a voltage dependent or a junction geometry dependent term only, while removing the unwanted terms. For the plasmon-modified hot electron thermal emission and the coherent multi-electron interaction model, the respective normalization eliminates the posited device dependent LSP resonance, leaving only the electron dynamics term which reflects crucial information about the microscopic process. In the finite temperature model, current noise which corresponds to the electron dynamics in producing the upconverted photons is scaled out at first, leaving (within that model) the device dependent LSP modes under further analysis. These methods offer an effective way in discerning the above-threshold contribution for each mechanism.

IV. CONCLUSIONS

Understanding the origin of above-threshold light emission in plasmonic tunnel junctions is critical in testing a variety of theoretical models and inspiring future work on engineering plasmonically active nanostructures for potential novel applications. Our experimental observations and theoretical analysis imply that plasmon-induced hot carrier recombination may play a dominant role over other possible candidates for the above-threshold light emission of a planar on-chip junction operating in a high current regime (~10 s to 100 s of μA under modest voltage bias). However, there are still outstanding challenges, overcoming which is key to bringing a complete picture to the plasmonic light emission phenomenon. Beyond existing simple analytical models, addressing the extreme scale light–matter interactions via rigorous quantitative first-principles calculation is a great challenge. A comprehensive picture of an open driven plasmonic system should incorporate carrier transport, inelastic electron–electron and electron–phonon interaction, elastic disorder and surface scattering, and interactions of electronic and plasmonic excitations. Furthermore, potential applications of the observed upconversion light emission, such as deep subwavelength photon sources or on-chip wireless communication, are currently limited by this process' poor energy conversion efficiency (significantly lower than that reported for below-threshold light emission[16,18]). Therefore, it is necessary to develop approaches to optimize the plasmonic properties of tunnel junctions as well as the hot-carrier generation and relaxation processes.[5] In addition, modulating the tunnel junctions via a tunable vacuum gap in a scanning probe configuration or applying self-assembled molecules to modify the plasmonic resonances and electronic properties[59,63–66] may also lead to potential applications in active plasmonic photochemistry.[19,42]

AUTHORS' CONTRIBUTIONS

D.N. and L.C. designed the experiment. Y.Z. and L.C. fabricated the devices, conducted the experiment, and modeled the data. All authors wrote the manuscript and have given approval to the final version of the manuscript.

ACKNOWLEDGMENTS

L.C. acknowledges funding support from the J. Evans Attwell Welch Fellowship, the Smalley Curl Institute at Rice University, and the support of University of Colorado at Boulder. D.N. and Y.Z. acknowledge the Robert A. Welch Foundation Award No. C-1636. D.N. acknowledges support from the National Science Foundation (NSF) under No. ECCS-1704625.

DATA AVAILABILITY

The data that support the findings of this study are available from the corresponding author upon reasonable request.

REFERENCES

[1]F. Benz, M. K. Schmidt, A. Dreismann, R. Chikkaraddy, Y. Zhang, A. Demetriadou, C. Carnegie, H. Ohadi, B. de Nijs, R. Esteban, J. Aizpurua, and J. J. Baumberg, Science **354**, 726 (2016).
[2]D. R. Ward, F. Hüser, F. Pauly, J. C. Cuevas, and D. Natelson, Nat. Nanotechnol. **5**, 732 (2010).
[3]R. Chikkaraddy, B. de Nijs, F. Benz, S. J. Barrow, O. A. Scherman, E. Rosta, A. Demetriadou, P. Fox, O. Hess, and J. J. Baumberg, Nature **535**, 127 (2016).
[4]C. C. Leon, A. Rosławska, A. Grewal, O. Gunnarsson, K. Kuhnke, and K. Kern, Sci. Adv. **5**, eaav4986 (2019).
[5]H. Reddy, K. Wang, Z. Kudyshev, L. Zhu, S. Yan, A. Vezzoli, S. J. Higgins, V. Gavini, A. Boltasseva, P. Reddy, V. M. Shalaev, and E. Meyhofer, Science **369**, 423 (2020).

[6]D. R. Ward, D. A. Corley, J. M. Tour, and D. Natelson, Nat. Nanotechnol. **6**, 33 (2011).
[7]H. Park, J. Park, A. K. L. Lim, E. H. Anderson, A. P. Alivisatos, and P. L. McEuen, Nature **407**, 57 (2000).
[8]A. Nitzan and M. A. Reed, Science **300**, 1384 (2003).
[9]S. V. Aradhya and L. Venkataraman, Nat. Nanotechnol. **8**, 399 (2013).
[10]D. Xiang, X. Wang, C. Jia, T. Lee, and X. Guo, Chem. Rev. **116**, 4318 (2016).
[11]L. Cui, R. Miao, C. Jiang, E. Meyhofer, and P. Reddy, J. Chem. Phys. **146**, 092201 (2017).
[12]L. Cui, W. Jeong, S. Hur, M. Matt, J. C. Klöckner, F. Pauly, P. Nielaba, J. C. Cuevas, E. Meyhofer, and P. Reddy, Science **355**, 1192 (2017).
[13]L. Cui, S. Hur, Z. A. Akbar, J. C. Klöckner, W. Jeong, F. Pauly, S.-Y. Jang, P. Reddy, and E. Meyhofer, Nature **572**, 628 (2019).
[14]J. Lambe and S. L. McCarthy, Phys. Rev. Lett. **37**, 923 (1976).
[15]M. Parzefall, P. Bharadwaj, A. Jain, T. Taniguchi, K. Watanabe, and L. Novotny, Nat. Nanotechnol. **10**, 1058 (2015).
[16]J. Kern, R. Kullock, J. Prangsma, M. Emmerling, M. Kamp, and B. Hecht, Nat. Photonics **9**, 582 (2015).
[17]S. P. Gurunarayanan, N. Verellen, V. S. Zharinov, F. James Shirley, V. V. Moshchalkov, M. Heyns, J. Van De Vondel, I. P. Radu, and P. Van Dorpe, Nano Lett. **17**, 7433 (2017).
[18]H. Qian, S.-W. Hsu, K. Gurunatha, C. T. Riley, J. Zhao, D. Lu, A. R. Tao, and Z. Liu, Nat. Photonics **12**, 485 (2018).
[19]P. Wang, A. V. Krasavin, M. E. Nasir, W. Dickson, and A. V. Zayats, Nat. Nanotechnol. **13**, 159 (2018).
[20]M. Parzefall, Á Szabó, T. Taniguchi, K. Watanabe, M. Luisier, and L. Novotny, Nat. Commun. **10**, 1 (2019).
[21]W. Du, T. Wang, H. S. Chu, and C. A. Nijhuis, Nat. Photonics **11**, 623 (2017).
[22]C. Zhang, J.-P. Hugonin, A.-L. Coutrot, C. Sauvan, F. Marquier, and J.-J. Greffet, Nat. Commun. **10**, 4949 (2019).
[23]K. S. Makarenko, T. X. Hoang, T. J. Duffin, A. Radulescu, V. Kalathingal, H. J. Lezec, H. Chu, and C. A. Nijhuis, Adv. Sci. **7**, 1900291 (2020).
[24]R. Faggiani, J. Yang, and P. Lalanne, ACS Photonics **2**, 1739 (2015).
[25]J. Yang, R. Faggiani, and P. Lalanne, Nanoscale Horiz. **1**, 11 (2016).
[26]F. Bigourdan, J.-P. Hugonin, F. Marquier, C. Sauvan, and J.-J. Greffet, Phys. Rev. Lett. **116**, 106803 (2016).
[27]R. Pechou, R. Coratger, F. Ajustron, and J. Beauvillain, Appl. Phys. Lett. **72**, 671 (1998).
[28]A. Downes, P. Dumas, and M. E. Welland, Appl. Phys. Lett. **81**, 1252 (2002).
[29]C. Ott, S. Götzinger, and H. B. Weber, Phys. Rev. Res. **2**, 042019 (2020).
[30]L. Cui, Y. Zhu, M. Abbasi, A. Ahmadivand, B. Gerislioglu, P. Nordlander, and D. Natelson, Nano Lett. **20**, 6067 (2020).
[31]G. Hoffmann, R. Berndt, and P. Johansson, Phys. Rev. Lett. **90**, 046803 (2003).
[32]G. Schull, N. Néel, P. Johansson, and R. Berndt, Phys. Rev. Lett. **102**, 057401 (2009).
[33]Z. C. Dong, X. L. Zhang, H. Y. Gao, Y. Luo, C. Zhang, L. G. Chen, R. Zhang, X. Tao, Y. Zhang, J. L. Yang, and J. G. Hou, Nat. Photonics **4**, 50 (2010).
[34]N. L. Schneider, G. Schull, and R. Berndt, Phys. Rev. Lett. **105**, 026601 (2010).
[35]M. Buret, A. V. Uskov, J. Dellinger, N. Cazier, M.-M. Mennemanteuil, J. Berthelot, I. V. Smetanin, I. E. Protsenko, G. Colas-des-Francs, and A. Bouhelier, Nano Lett. **15**, 5811 (2015).
[36]P.-J. Peters, F. Xu, K. Kaasbjerg, G. Rastelli, W. Belzig, and R. Berndt, Phys. Rev. Lett. **119**, 066803 (2017).
[37]E. Ekici, P. Kapitza, C. A. Bobisch, and R. Möller, Opt. Lett. **42**, 4585 (2017).
[38]V. Kalathingal, P. Dawson, and J. Mitra, Sci. Rep. **7**, 3530 (2017).
[39]R. Kullock, M. Ochs, P. Grimm, M. Emmerling, and B. Hecht, Nat. Commun. **11**, 115 (2020).
[40]P. Christopher, H. Xin, and S. Linic, Nat. Chem. **3**, 467 (2011).
[41]E. Cortés, W. Xie, J. Cambiasso, A. S. Jermyn, R. Sundararaman, P. Narang, S. Schlücker, and S. A. Maier, Nat. Commun. **8**, 14880 (2017).
[42]L. Zhou, D. F. Swearer, C. Zhang, H. Robatjazi, H. Zhao, L. Henderson, L. Dong, P. Christopher, E. A. Carter, P. Nordlander, and N. J. Halas, Science **362**, 69 (2018).
[43]Y. Li, P. Doak, L. Kronik, J. B. Neaton, and D. Natelson, Proc. Natl. Acad. Sci. U.S.A. **111**, 1282 (2014).
[44]Y. Li, P. Zolotavin, P. Doak, L. Kronik, J. B. Neaton, and D. Natelson, Nano Lett. **16**, 1104 (2016).
[45]S. Kaneko, K. Yasuraoka, and M. Kiguchi, J. Phys. Chem. C **123**, 6502 (2019).
[46]M. W. Knight, H. Sobhani, P. Nordlander, and N. J. Halas, Science **332**, 702 (2011).
[47]W. Li, Z. J. Coppens, L. V. Besteiro, W. Wang, A. O. Govorov, and J. Valentine, Nat. Commun. **6**, 8379 (2015).
[48]A. Lay, D. S. Wang, M. D. Wisser, R. D. Mehlenbacher, Y. Lin, M. B. Goodman, W. L. Mao, and J. A. Dionne, Nano Lett. **17**, 4172 (2017).
[49]N. L. Schneider, P. Johansson, and R. Berndt, Phys. Rev. B **87**, 45409 (2013).
[50]H. Park, A. K. L. Lim, A. P. Alivisatos, J. Park, and P. L. McEuen, Appl. Phys. Lett. **75**, 301 (1999).
[51]N. J. Halas, S. Lal, S. Link, W.-S. Chang, D. Natelson, J. H. Hafner, and P. Nordlander, Adv. Mater. **24**, 4842 (2012).
[52]J. B. Herzog, M. W. Knight, Y. Li, K. M. Evans, N. J. Halas, and D. Natelson, Nano Lett. **13**, 1359 (2013).
[53]W. Zhu, R. Esteban, A. G. Borisov, J. J. Baumberg, P. Nordlander, H. J. Lezec, J. Aizpurua, and K. B. Crozier, Nat. Commun. **7**, 11495 (2016).
[54]J. Aizpurua, G. Hoffmann, S. P. Apell, and R. Berndt, Phys. Rev. Lett. **89**, 156803 (2002).
[55]D. Zhang, X. Zheng, and M. Di Ventra, Phys. Rep. **830**, 1 (2019).
[56]J. G. Liu, H. Zhang, S. Link, and P. Nordlander, ACS Photonics **5**, 2584 (2018).
[57]F. Xu, C. Holmqvist, and W. Belzig, Phys. Rev. Lett. **113**, 066801 (2014).
[58]K. Kaasbjerg and A. Nitzan, Phys. Rev. Lett. **114**, 126803 (2015).
[59]F. Xu, C. Holmqvist, G. Rastelli, and W. Belzig, Phys. Rev. B **94**, 245111 (2016).
[60]Y. M. Blanter and M. Büttiker, Phys. Rep. **336**, 1 (2000).
[61]R. W. Rendell and D. J. Scalapino, Phys. Rev. B **24**, 3276 (1981).
[62]J. G. Simmons, J. Appl. Phys. **34**, 1793 (1963).
[63]S. F. Tan, L. Wu, J. K. W. Yang, P. Bai, M. Bosman, and C. A. Nijhuis, Science **343**, 1496 (2014).
[64]L. Cui, W. Jeong, V. Fernández-Hurtado, J. Feist, F. J. García-Vidal, J. C. Cuevas, E. Meyhofer, and P. Reddy, Nat. Commun. **8**, 14479 (2017).
[65]E. Kazuma, J. Jung, H. Ueba, M. Trenary, and Y. Kim, Science **360**, 521 (2018).
[66]L. Cui, R. Miao, K. Wang, D. Thompson, L. A. Zotti, J. C. Cuevas, E. Meyhofer, and P. Reddy, Nat. Nanotechnol. **13**, 122 (2018).